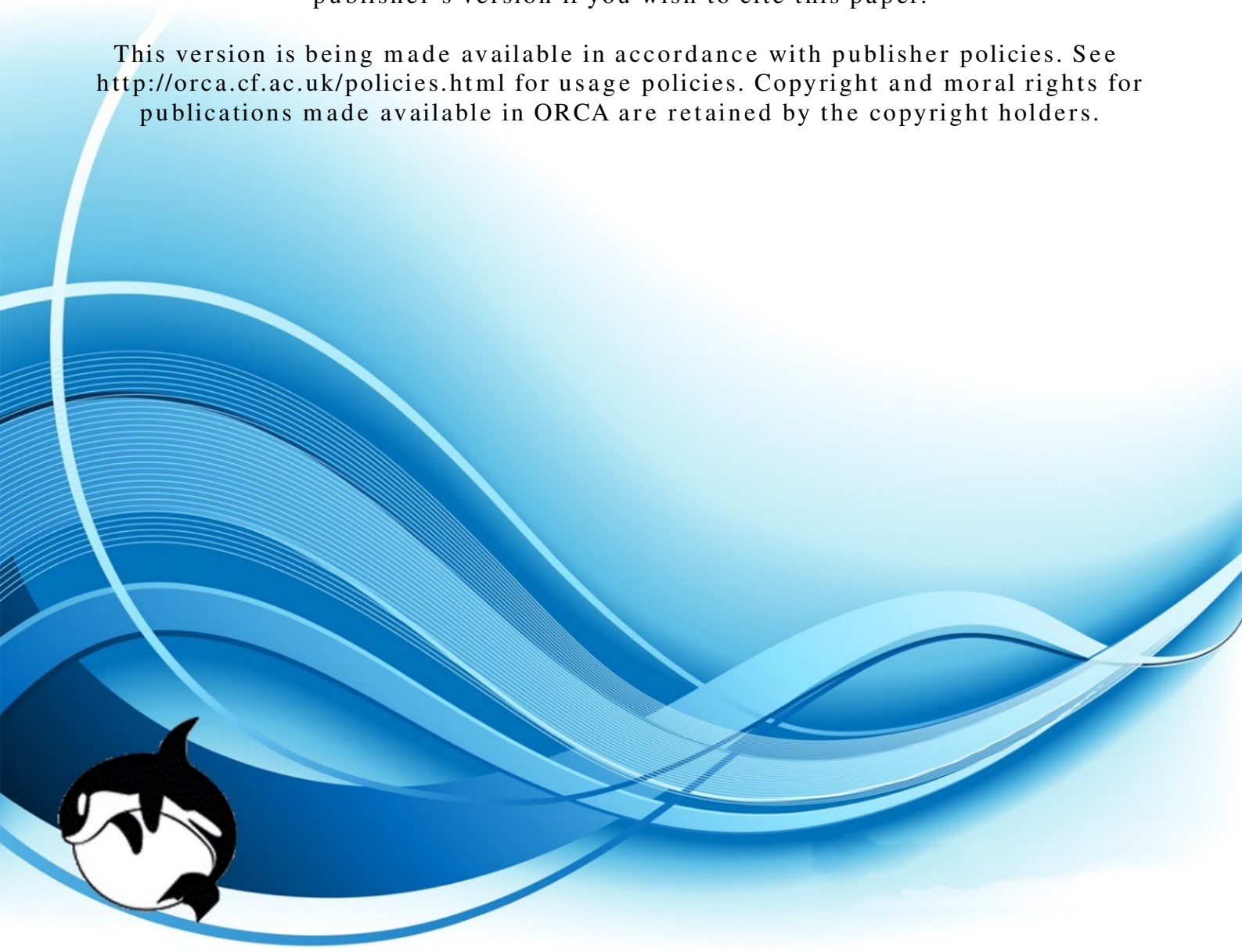

Heterogeneity Induces Spatiotemporal Oscillations in Reaction-Diffusions Systems

Andrew L. Krause[1,*], Václav Klika[1,2], Thomas E. Woolley[3], and Eamonn A. Gaffney[1]
[1] *Mathematical Institute, University of Oxford, Andrew Wiles Building, Radcliffe Observatory Quarter, Woodstock Road, Oxford, OX2 6GG, United Kingdom*
[2] *Department of Mathematics, FNSPE, Czech Technical University in Prague, Trojanova 13, 120 00 Praha, Czech Republic and*
[3] *Cardiff School of Mathematics, Cardiff University, Senghennydd Road, Cardiff, CF24 4AG, United Kingdom*

We report on a novel instability arising in activator-inhibitor reaction-diffusion (RD) systems with a simple spatial heterogeneity. This instability gives rise to periodic creation, translation, and destruction of spike solutions that are commonly formed due to Turing instabilities. While this behavior is oscillatory in nature, it occurs purely within the Turing space such that no region of the domain would give rise to a Hopf bifurcation for the homogeneous equilibrium. We use the shadow limit of the Gierer-Meinhardt system to show that the speed of spike movement can be predicted from well-known asymptotic theory, but that this theory is unable to explain the emergence of these spatiotemporal oscillations. Instead, we numerically explore this system and show that the oscillatory behavior is caused by the destabilization of a steady spike pattern due to the creation of a new spike arising from endogeneous activator production. We demonstrate that on the edge of this instability, the period of the oscillations goes to infinity, although it does not fit the profile of any well known bifurcation of a limit cycle. We show that nearby stationary states are either Turing unstable, or undergo saddle-node bifurcations near the onset of the oscillatory instability, suggesting that the periodic motion does not emerge from a local equilibrium. We demonstrate the robustness of this spatiotemporal oscillation by exploring small localized heterogeneity, and showing that this behavior also occurs in the Schnakenberg RD model. Our results suggest that this phenomenon is ubiquitous in spatially heterogeneous RD systems, but that current tools, such as stability of spike solutions and shadow-limit asymptotics, do not elucidate understanding. This opens several avenues for further mathematical analysis and highlights difficulties in explaining how robust patterning emerges from Turing's mechanism in the presence of even small spatial heterogeneity.

I. MOTIVATION FOR REACTION-DIFFUSION IN HETEROGENEOUS MEDIA

Since Turing's pioneering work on morphogenesis [1], a considerable amount of research has explored the tremendous power of reaction-diffusion (RD) models to generate patterns in time and space. In particular, RD systems can give rise to a huge variety of emergent stationary patterns, as well as spatiotemporal dynamics. Despite the success of the theory at capturing the attention of scientists for many decades, there are still fundamental obstructions to utilizing the reaction-diffusion framework to help explain processes in developmental biology [2]. An important example of this, presaged by Turing himself, is that most patterning processes of interest do not emerge from homogeneous equilibrium states, but instead evolve in complex spatial settings, and especially from previous patterning processes. To quote Turing [1], "Most of an organism, most of the time is developing from one pattern into another, rather than from homogeneity into a pattern." While there has been some research investigating the role of spatial heterogeneity on reaction-diffusion theory, we demonstrate here that novel dynamical phenomena exist which have hitherto been unreported, even for simple two-component reaction-diffusion equations.

Explicit spatial heterogeneity has been incorporated into reaction-diffusion theory in many contexts, such as chemical pre-patterns in developmental biology [3], environmental heterogeneity in collective animal dispersal [4], reaction-diffusion models with non-isotropic growth [5], as well as in models with differential diffusion leading to spatial inhomogeneity, such as in plant root initiation [6, 7]. In the developmental setting, heterogeneity has been suggested as extremely important for organising different regions along cell boundaries based on sharp variations in gene expression [8, 9]. Spatial heterogeneity has been shown to change local instability conditions for pattern formation [10, 11], modulate size and wavelength of patterns [12], and localize (or pin) spike patterns in space [13–16]. We also note that

* krause@maths.ox.ac.uk

the presence of immobile substrates can induce spatiotemporal behavior as the local environment evolves, leading to changes in the stability of equilibria [17, 18], although these approaches introduce a third component in the system which gives rise to model complexity not present in the two-component case. Bifurcation structures of reaction-diffusion equations with spatial heterogeneity have been studied as far back as the 1970s [19] where heterogeneity was discussed in the context of open thermodynamic systems and dissipative structures.

In this paper our objective is to demonstrate that simple forms of heterogeneity can induce spatiotemporal oscillations in two-component reaction-diffusion systems away from Hopf bifurcations or other known oscillation-inducing mechanisms. We show that while this behavior can depend on the details of the system (e.g. the reaction kinetics, boundary conditions, and size of the domain), it can easily be produced in a variety of model systems with a substantial robustness to these details. The robustness and ubiquity of this non-equilibrium behavior has implications for a variety of applications of reaction-diffusion theory where spatial heterogeneity itself is ubiquitous, such as in modeling animal dispersal [20, 21] or in developmental settings [22]. In these realistic settings, the homogeneous theory is a crude mathematical abstraction that may not recapitulate qualitatively different spatiotemporal dynamics induced by the presence of spatial heterogeneity.

We remark that similar dynamical behaviors have been found in other reaction-diffusion systems, but these have typically been driven by specific nonlinearities and do not have the same simple forms of heterogeneity that we have explored here. For instance, the authors in [23] demonstrate oscillatory and chaotic dynamics in a (spatially homogeneous) reaction-diffusion system that is not captured by local (linear) analysis, although an analysis of the underlying reaction kinetics suggests that a nonlinear analysis of the homogeneous ODE system explains the origin of their results. In [24], the authors asymptotically and numerically explored the Gray-Scott model to demonstrate drift and oscillatory instabilities in one and two spike solutions, but the long-time dynamics of these spikes are relatively tame in the asymptotic regime they consider (corresponding to pinning in a particular region of the domain, or disappearing due to instability).

Traveling waves and pulses have also been studied in heterogeneous media extensively [25–27]. In particular, a number of studies, for instance [28–30], have considered heterogeneity-induced defects in three-component reaction-diffusion systems, some of which have a qualitatively similar structure to the dynamics reported here. However, these studies involve specific reaction kinetics in three-component systems, and the traveling wave solutions obtained do not have the same recurrent trajectories as those presented here. Several authors have also investigated travelling-wave patterns created via spatiotemporal forcing, especially in the context of photosensitive CDIMA reactions [31–33]. Finally, we mention that traveling waves and other dynamical phenomena are often studied in reaction-advection-diffusion systems, and that many recent authors have included various forms of spatial heterogeneity into such models [34–36]. In [37] advection induces periodic creation, translation, and destruction of localized patterns, where the spatiotemporal behavior is qualitatively similar to what we observe in this paper. We show here, however, that we expect such periodic motions to be generic in reaction-diffusion systems with spatial heterogeneity without relying on the presence of advection to induce pattern movement.

II. OSCILLATING SPATIOTEMPORAL PATTERNS

We begin by considering the non-dimensional Gierer-Meinhardt [38] equations in the form,

$$\frac{\partial u}{\partial t} = r\left(\alpha + \frac{u^2}{v}\right) - \left(\mu + c_m H\left(\frac{x}{L_x}\right)\right)u + \nabla^2 u, \quad \frac{\partial v}{\partial t} = ru^2 - \left(\nu + c_n H\left(\frac{x}{L_x}\right)\right)v + d\nabla^2 v, \tag{1}$$

with all parameters positive, $x \in [0, L_x]$, and with given initial data $u(x,0) = u_0(x)$ and $v(x,0) = v_0(x)$. Here u and v are the concentrations of activator and inhibitor respectively; α is the feed rate; μ and ν are the degradation rates of the activator and inhibitor; L_x is the domain size; d is the ratio of diffusion coefficients; c_m and c_n are the magnitudes of the spatial heterogeneity in the activator and inhibitor equation respectively, and H is the functional form of the heterogeneity, which takes an input from $[0, 1]$ and returns a value in the same interval. We consider both a linear function $H(x) = x$, as well as a 'localised' heterogeneity $H(x) = (1 + \tanh(G(x - 1/2)))/2$, where $G > 1$ is a smoothing parameter such that H approaches a step function at the midpoint of the domain in the limit of $G \to \infty$.

We numerically integrated (1) using the commercially-available finite element software COMSOL v5.3a with 10^4 second-order elements and absolute and relative tolerances of 10^{-5}. We used small random initial conditions given by $u_0(x) = |0.01+\xi(x)|$ and $v_0(x) = |0.01+\zeta(x)|$ where ξ and ζ are normally distributed with zero mean and a variance of

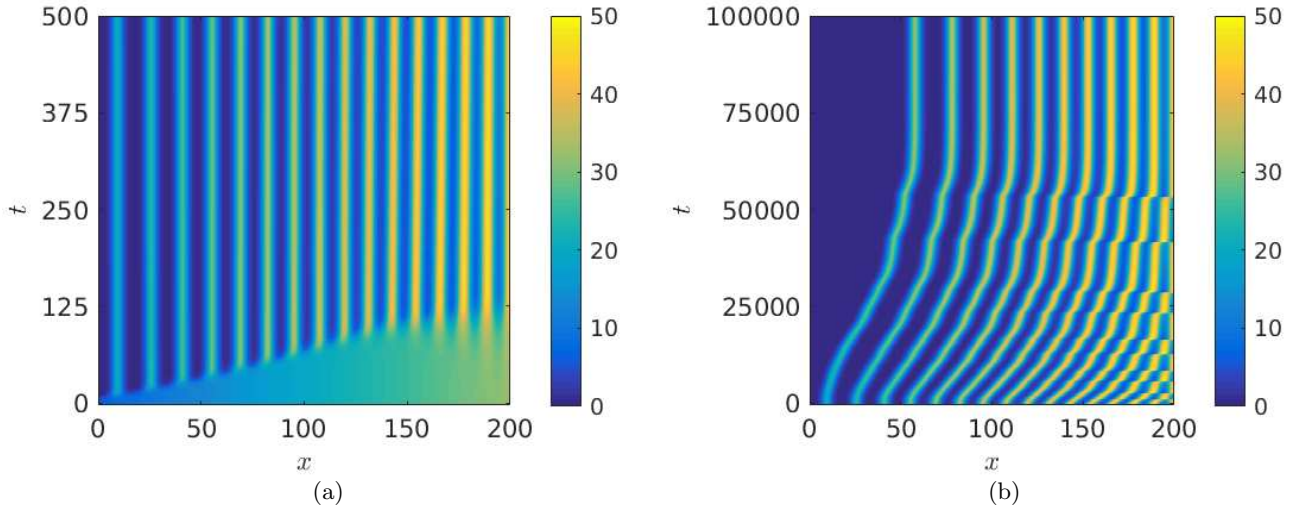

(a) (b)

FIG. 1: Plots of u over space and time from a solution to (1) with $r = 1$, $d = 200$, $L_x = 200$, $\mu = 0.8$, $\nu = 5.5$, $\alpha = 0$ with $c_m = 0$ and $c_n = 20$. We set $H(x) = x$ and used homogeneous Neumann boundary conditions (Color Figures available online).

10^{-4}. We also ran each simulation with perturbations from the uniform steady state, taking $u_0(x) = |(\alpha r+\nu)/\mu+\xi(x)|$ and $v_0(x) = |(r(\alpha r+\nu)^2)/(\mu^2\nu)+\zeta(x)|$, and observed no differences in the long-time behavior. We have checked each simulation using 18 other realizations of the initial condition to confirm long-time behavior, and also ran simulations for longer time periods than shown in the results to confirm we were observing long-time asymptotic behavior. Additionally, we checked the convergence of our numerical solutions by implementing solvers in both Mathematica and Matlab (using finite-differences), and obtained identical results (within numerical precision) for the same initial data.

We first demonstrate the effect of the heterogeneity on localized spike solutions to Equation (1) in the case of $\alpha = 0$, which is the most widely-studied case in the literature. In Figure 1a we see that spikes form on a timescale of $O(10^2)$, and that the spikes have a (heterogeneous) wavelength as shown in [12]. Over longer timescales ($O(10^4)$), we see from Figure 1b that these spikes travel along the heterogeneity as described in [14], and that spikes at the rightmost boundary disappear as other spikes move toward that boundary. This movement and subsequent instability occurs on a much longer timescale than the spike formation, so that it would be quite easy to mistake the final distribution in Figure 1a as a steady state solution to (1). We note that the actual steady state solution shown at the end of Figure 1b has several qualitative differences with the transient solution in Figure 1a in terms of number and wavelength of spikes. For $\alpha \lesssim 10^{-2}$, qualitatively similar behavior occurs, with the only difference being the formation of a small boundary spike at the leftmost boundary (such as in Figures 2a or 4a). However, for larger values of α, we observe spatiotemporal oscillations, which we now describe in detail.

In Figure 2 we show simulations of equation (1) in a 1-D domain with Neumann boundary conditions and a linear heterogeneity only in the activator ($H(x) = x$, $c_n = 0$). In Figure 2a color denotes the value of the activator u with space along the horizontal axis and time along the vertical axis, whereas in Figure 2b we show the evolution of the solution profile for a short period of time across the domain for the same simulation. Spatially localized 'spikes' form, which is typical for large values of d in the Gierer-Meinhardt system, but these immediately undergo a complicated transient behavior before settling onto a long-time spatiotemporal oscillation. This oscillation consists of translation of each spike solution, and an instability which leads to the destruction of the spike near one end of the domain; this is visible in the leftmost interior spike of Figure 2b which decays rapidly as the nearby spike approaches it. On the opposite (right) side of the domain, a new spike forms and begins traveling along the heterogeneity, continuing the process. We remark that we observe comparable behavior with Dirichlet boundary conditions, as well as in wide regions of the parameter space in this system.

In Figure 3, we demonstrate two more examples of space-time solutions for the same parameter values and boundary conditions as in Figure 2, but using the above-mentioned tanh function to create a step heterogeneity, which localizes spatial variation in the domain to a small subregion near the midpoint. We see that the interior spikes move as before in the gradient of the heterogeneity, but that the creation and destruction of spikes is now clearly inside of the domain

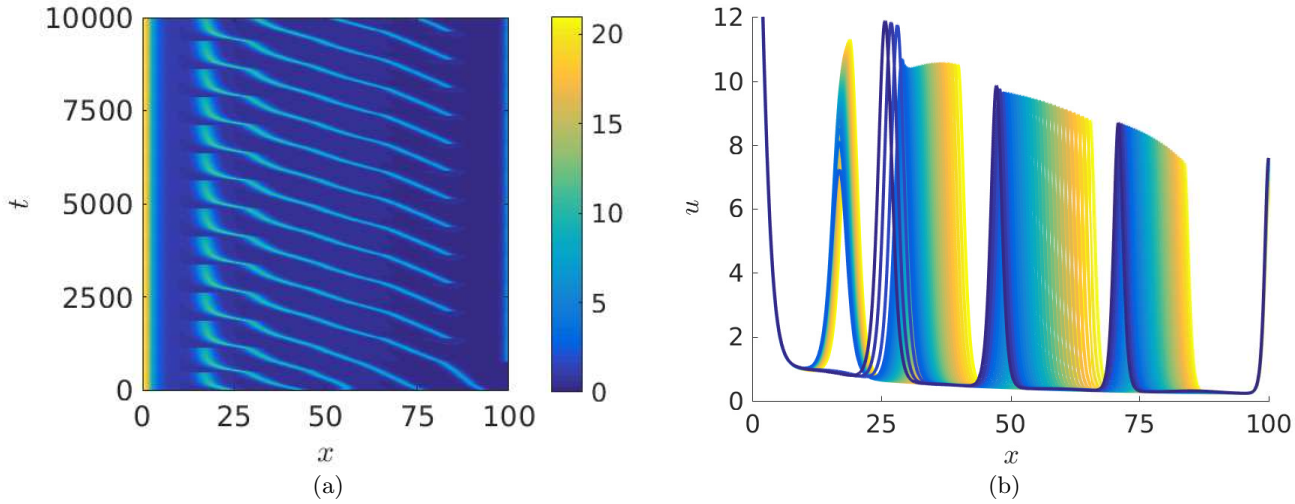

(a) (b)

FIG. 2: Solutions to (1) with $r = 1$, $d = 200$, $L_x = 100$, $\mu = 0.8$, $\nu = 5.5$, $\alpha = 1$ with $c_m = 4$ and $c_n = 0$. We set $H(x) = x$ and used homogeneous Neumann boundary conditions. In (a) we plot the value of u over time and space. In (b) we plot a (colored) spatial profile at a sequence of times from $t = 8900$ in yellow (light gray, to the right) to $t = 9440$ in blue (darker, to the left) (Color Figures available online).

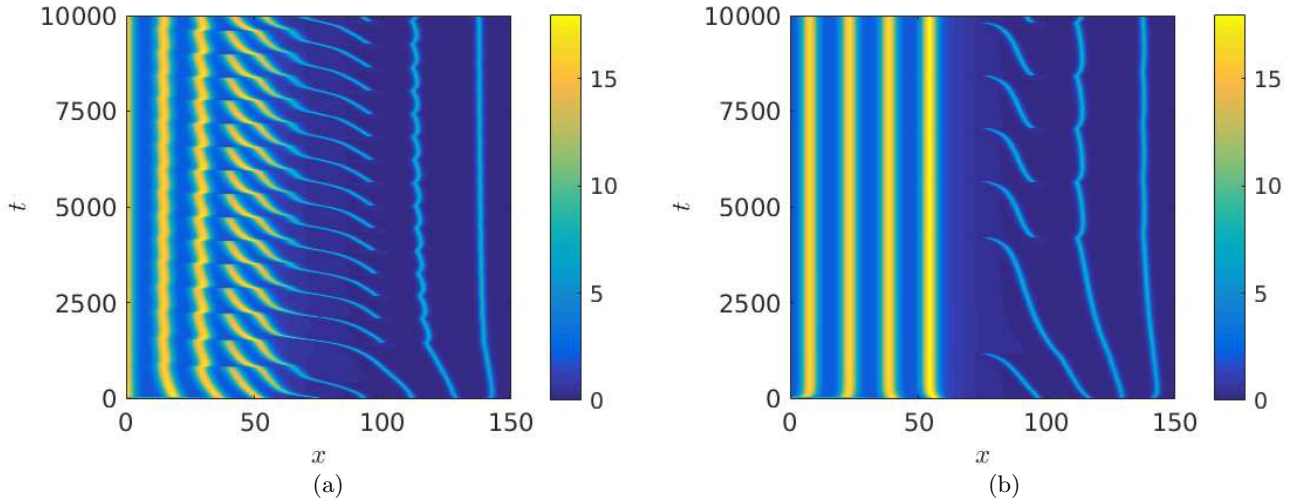

(a) (b)

FIG. 3: Plots of u over space and time from solutions to (1) with $r = 1$, $d = 200$, $L_x = 150$, $\mu = 0.8$, $\nu = 5.5$, $\alpha = 1$ with $c_m = 4$ and $c_n = 0$. We set $H(x) = (1 + \tanh(G(x - 1/2)))/2$ with $G = 10$ in (a) and $G = 17$ in (b) and used homogeneous Neumann boundary conditions in both cases (Color Figures available online).

and separated from the boundaries. In particular, in Figure 3b, we see that a single spike forms and is destroyed before a new spike has developed to a comparable amplitude. We note that the spike to the right of this periodically moving spike plays a role in its creation and destruction, and is similarly pushed back when a new spike is formed due to non-local interactions mediated by the rapidly-diffusing inhibitor.

This behavior exists in large regions of the parameter space for Gierer-Meinhardt, even using other variants of the heterogeneity. In Figure 4a, we demonstrate this using only a linear heterogeneity in the inhibitor ($c_m = 0$), and in Figure 4b we exhibit such an oscillation where the spatial variation is 10% of the effective parameter it is modifying (namely, the parameter μ which corresponds to degradation of the activator). We note that this second example is also over a very large domain with many spikes, so that the spatial variation in parameters between neighboring spikes is in fact much less than 1%, and yet this oscillatory behavior persists. In most parameter regimes that we explored, the spatial heterogeneity (the magnitude of c_m or c_n) or the basal production rate (α) needed to be large enough to

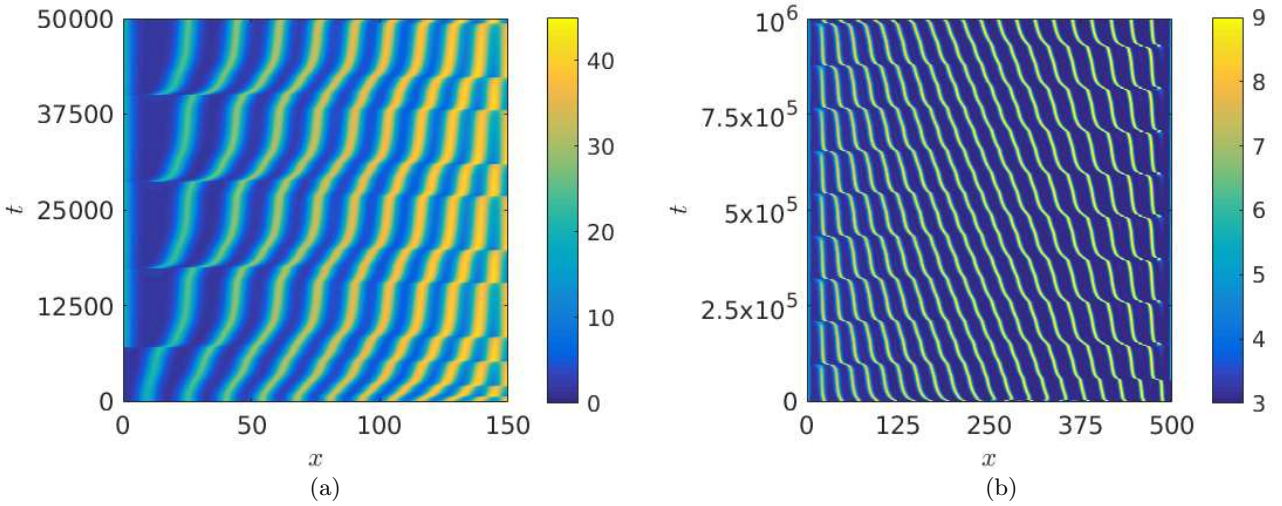

FIG. 4: Plots of u over space and time from solutions to (1) with $d = 200$, $L_x = 150$, $\mu = 0.8$, $\nu = 5.5$, $\alpha = 1$, $c_m = 0$ and $c_n = 17$ in (a), and $d = 400$, $L_x = 500$, $\mu = 1.5$, $\nu = 4$, $\alpha = 2.8$, $c_n = 0$ and $c_m = 0.15$ in (b). In both cases we set $r = 1$, $H(x) = x$, and used homogeneous Neumann boundary conditions (Color Figures available online).

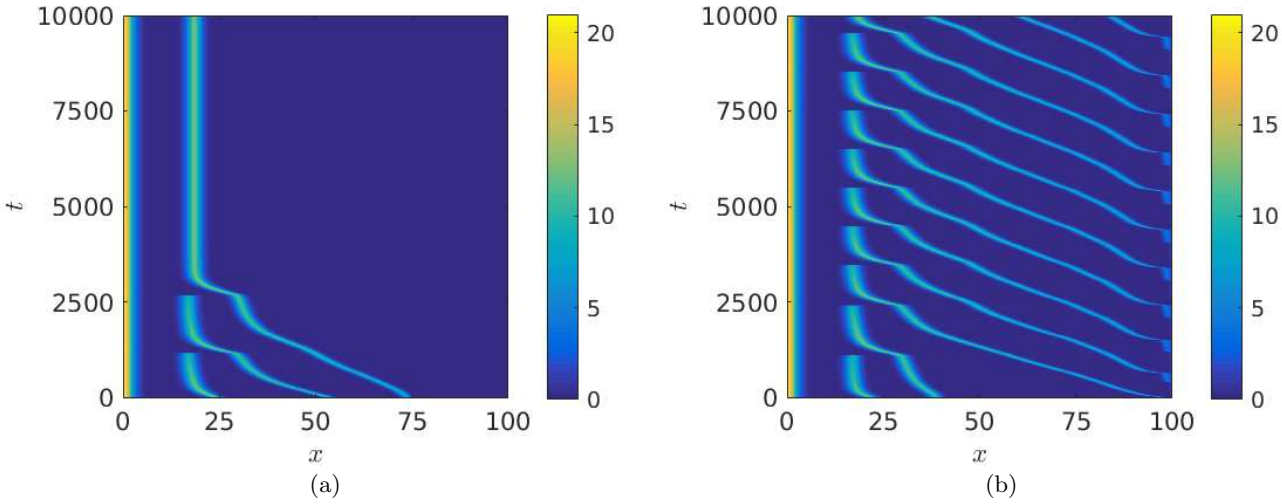

FIG. 5: Plots of u over space and time from solutions to (1) with $d = 200$, $L_x = 100$, $\mu = 0.8$, $\nu = 5.5$, $\alpha = 0$, $c_m = 4$ and $c_n = 0$ in (a) and (b). In both cases we set $r = 1$, $H(x) = x$, and used homogeneous Neumann boundary conditions in (a), and an inhomogeneous Dirichlet condition of $u = u^* \approx 1.3$ in (b) for only the right boundary (Color Figures available online).

induce these kinds of oscillations, but it was not difficult to produce a large variety of examples as long as parameters were chosen from the Turing space so that patterning occurred.

We give one further set of example simulations demonstrating the role of activator production, which is necessary for new spikes to form. In Figure 5a, we set $\alpha = 0$ using the same parameters as in Figure 2a, and observe spike movement and destruction, but no formation of new spikes. In Figure 5b, we change the rightmost boundary condition for the activator to be an inhomogeneous Dirichlet condition, so that $u = u^*$ at that point, where u^* is the homogeneous steady state solution. In this case, the boundary source is sufficient to induce a spot to form and travel along the heterogeneity, producing a qualitatively comparable picture to Figure 2a. This provides us with a reasonable explanation of the mechanism underlying these oscillations. The heterogeneity drives spikes in a particular direction, spike-spike interactions destabilize an individual spike, leaving room for further traveling, and finally enough room is left to generate a new spike pattern inducing this recurrent behavior.

We note that the movement of the spikes is always toward the minimum of H in the case of $c_n = 0$, or its maximum

in the case of $c_m = 0$, which is consistent with the dynamics of a single spike reported in [13, 14]; see, for instance, equation (2.25) of [14]. We proceed to assess the conjecture that the emergence of a new spike drives the traveling spike farthest away from it to become unstable and subsequently annihilated, due to local spike-spike interactions pushing one another in the same direction. This is evidenced by the observation that for significantly smaller values of the heterogeneity (c_m or c_n), transient spike movement and instability are observed, but a stationary pattern is reached where spike amplitude and wavelength variation exists throughout the domain, as in Figure 1b. Similarly, if the localized heterogeneity does not span a large enough part of the domain (setting $G = 18$ in Figure 3 for instance), then the spikes will reach stationary values on either side of the boundary, but will not interact across it. Finally, we also mention that the basal production of activator, via the parameter α, plays an important role in this behavior. If α is sufficiently small, a new spike will not form in the region left behind from the traveling spikes, as seen in Figure 1a.

III. BIFURCATIONS OF LIMIT CYCLES AND NON-UNIFORM EQUILIBRIA

We now consider the feeding-rate α, representing basal production of the activator, in relation to the spatiotemporal oscillations demonstrated above. In Figure 6a-b we plot solutions to (1) in a smaller domain for decreasing values of α. As before, we observe spike formation, movement, and destruction of the interior spikes. As α is decreased, there is an increased period between the formation of a new spike, and the destabilization of the previous one. For $\alpha < 0.34886$, a second interior spike does not form and the first remains stationary indefinitely (as in Figure 5a). In Figure 6c, we plot several numerically computed values of the period of the oscillations, denoted by P, and fit these to a power law which diverges to infinity at a critical value, α^*, so that $P \propto |\alpha - \alpha^*|^{-0.0945}$. We have numerically estimated that $\alpha^* \approx 0.348861$ where the periodic solution disappears (i.e. we do not observe it for any smaller value of α). We note that our numerically computed value of α^* changes marginally if different spatial discretizations are used, but for a given number of finite elements, we observe consistent dynamics for $\alpha > \alpha^*$ and $\alpha < \alpha^*$, and refer the reader to [39, 40] for discussion of finite approximations to infinite-dimensional bifurcation phenomena. We now consider the stability of the steady state for smaller values of α in order to get a sense of this phenomenon from both sides of this infinite-period bifurcation.

To explore the behavior of equilibria in this system, we discretize Equations (1) using second-order finite differences with 10^3 grid points, and consider this large (but finite-dimensional) dynamical system parameterized by α. We first solve Equations (1), using the same parameters as in Figure 6, for $\alpha = 0.348$ until the solution is approximately at a steady state. We then solve the time-independent algebraic system to accurately approximate the steady state using the Matlab function 'fsolve' with a function tolerance of 10^{-14}. We iteratively increase the value of α in steps of $\Delta\alpha = 10^{-6}$ and solve for the steady state at each step, using the previous steady state solution as an initial guess to the algebraic solver. We track the eigenvalues of the Jacobian of the system as α is varied. This procedure is commonly known as natural parameter continuation [41]. The values of the steady state and the eigenvalues of the Jacobian appear to change continuously as α is varied, so we are confident the steady state remains on the same solution branch as we continue the solution in α. Note that the discretization used here for continuation purposes differs with the finite element solver used throughout the rest of the paper, namely using finite differences and fewer discrete points. This leads to small differences in the critical value of α^* corresponding to the divergence of the period of the oscillation, and the value at which the steady state undergoes a bifurcation. However, these are always extremely close in all cases we investigated.

For $\alpha \leq 0.349$, the numerically continued solution is locally stable (all eigenvalues of the Jacobian have negative real part). At $\alpha \approx 0.3494848$, one eigenvalue of the Jacobian approaches 0 along the real axis, whereas the others are bounded away from the imaginary axis. Numerically the largest eigenvalue of the Jacobian evaluated at this steady state is $\lambda_1 \approx -10^{-7}$, and the next is $\lambda_2 \approx -2 \times 10^{-2}$. For smaller values of α, we use a deflation technique [42] to find another nearby steady state coexisting with the stable one. We determine that this other steady state is unstable. For larger values of α, we do not detect any nearby steady state solutions, suggesting that these steady states have hit an annihilation point. As only one eigenvalue approaches the imaginary axis with no imaginary part, this equilibrium does not undergo a Hopf bifurcation in this spatially discretized system; nevertheless, after the bifurcation point, the only observed trajectory is the spatiotemporal oscillation observed previously. These results provide numerical evidence for a saddle-node bifurcation occurring as α is increased.

We also consider varying α when the heterogeneity is only present in the inhibitor of the Gierer-Meinhardt system.

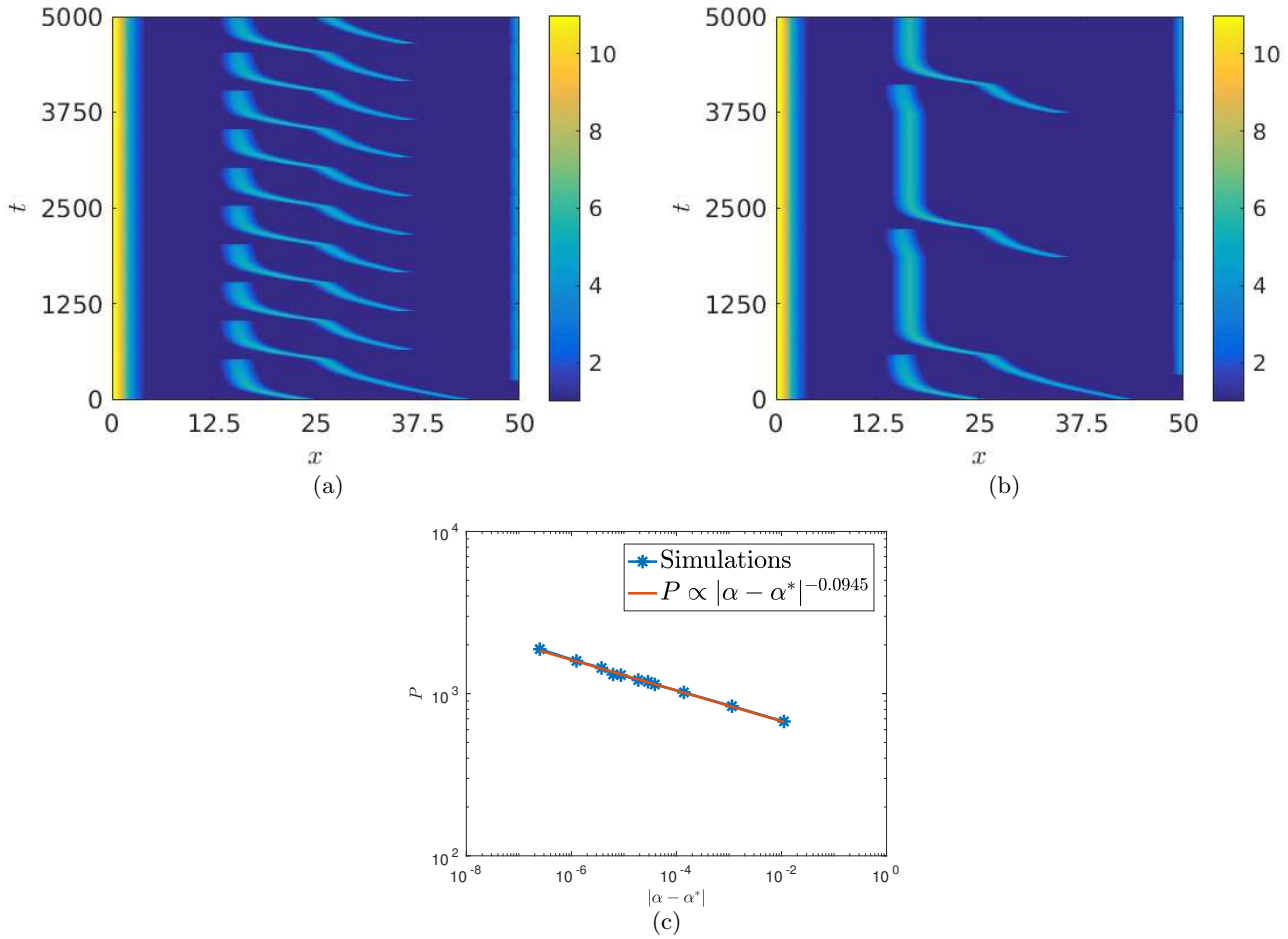

FIG. 6: Space-time plots of the activator u from solutions to Equations (1) in (a)-(b), and a logarithmic plot of the period of the oscillations P against α in (c) for a power law fit with $\alpha^* \approx 0.348861$. For all simulations we used $r = 1$, $d = 100$, $L_x = 50$, $\mu = 1$, $\nu = 4$, $c_m = 4$, $c_n = 0$, and in (a) $\alpha = 0.5$, and (b) $\alpha = 0.3488615$. In all cases, homogeneous Neumann boundary conditions are used (Color Figures available online).

We again demonstrate a divergence of the period of the oscillation in Figure 7, although the exponent of the power law (as well as the location of the critical value of α) are different in this case compared to in Figure 6. In this case we estimate a critical value of $\alpha^* \approx 2.8282965$. Performing the same continuation steps as in the previous case, we numerically predict a saddle-node bifurcation which occurs around $\alpha \approx 2.8267451$, where again we note the difference in the discretization schemes. As before, the largest eigenvalues are all negative and real, and the largest approaches zero much more quickly than the next-largest, with $\lambda_1 \approx -5 \times 10^{-6}$ and $\lambda_2 \approx -3 \times 10^{-2}$ at this value of α.

Similarly, we can consider the Schnakenberg equations in the form,

$$\frac{\partial u}{\partial t} = \alpha - u + u^2 v + c_m \frac{x}{L_x} u + \nabla^2 u, \quad \frac{\partial v}{\partial t} = \beta - u^2 v + d\nabla^2 v, \tag{2}$$

with all parameters positive (α again representing the feed rate of the activator, and β that of the inhibitor). Here we only consider one (linear) heterogeneity in the activator, but analogous behavior with heterogeneity in the inhibitor equation can be demonstrated.

We plot space-time solutions and the divergence of the period as α changes in Figure 8. We estimate an exponent for the power law, with a critical value of $\alpha^* \approx 1.13025$. We note that here the spatiotemporal behavior exists for $\alpha < \alpha^*$, and disappears at this critical value in the opposite way from the two examples given in the case of Gierer-Meinhardt kinetics. Using numerical continuation as in the previous cases, we numerically predict a saddle-node bifurcation which occurs around $\alpha \approx 1.13432$, where again we note the difference in the discretization schemes. As before, the

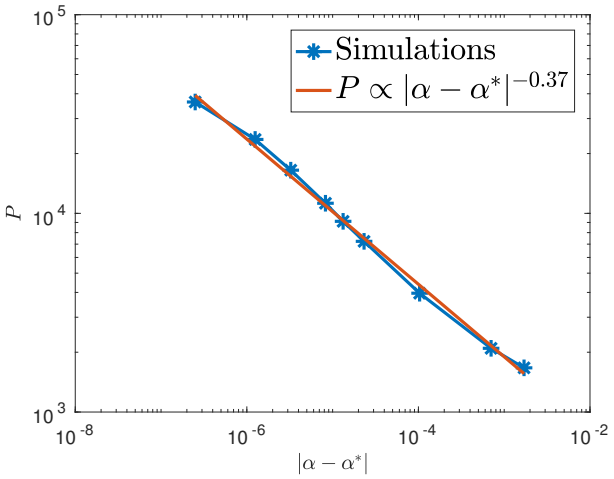

FIG. 7: A logarithmic plot of the period of the oscillations P against $|\alpha - \alpha^*|$ corresponding to solutions of (1) with $\alpha^* \approx 2.8282965$. For all simulations we used $r = 1$, $d = 200$, $L_x = 35$, $\mu = 1.5$, $\nu = 10$, $c_m = 0$, and $c_n = 35$ with homogeneous Neumann boundary conditions (Color Figures available online).

largest eigenvalues are all negative and real, and the largest approaches zero much more quickly than the next-largest, with $\lambda_1 \approx -9 \times 10^{-6}$ and $\lambda_2 \approx -9 \times 10^{-3}$ at this value of α.

The oscillation period data shown in Figures 6-8 are not reasonably fit with a logarithm of $|\alpha - \alpha^*|$, whereas they are all well-approximated by power laws, although with different exponents. Firstly, this suggests that this bifurcation is not a universal phenomenon, in the sense of critical phenomena in statistical physics, and secondly that it is not predicted to fit the profile of the two commonly-known codimension-1 bifurcations of limit cycles with periods tending to infinity. Specifically, a homoclinic bifurcation of a limit cycle would give the period P near the bifurcation point α^* the form $P \propto |\alpha - \alpha^*|^{-\frac{1}{2}}$, whereas a Blue Sky Catastrophe would diverge logarithmically as $P \propto -\ln(|\alpha - \alpha^*|)$ [43].

The critical value of α^* where the period of the oscillations was predicted to diverge differs slightly from the value of α where the non-uniform equilibrium undergoes a saddle-node bifurcation, but this difference is very likely due to the spatial discretizations used, and these bifurcations appear to occur at approximately the same value of α (the relative difference between these values is less than 0.4% in each case). To confirm this, we integrated the same discretization used in the continuation results to show that the value of the saddle-node bifurcation has the same qualitative properties as α^*; that is, on one side of this bifurcation point, solutions tend to the non-uniform steady state which we used in the numerical continuation; on the other side, solutions exhibit this oscillatory behavior. This is a peculiar result, as a saddle-node bifurcation is a purely local phenomenon and does not generate a limit cycle. Similarly, a limit cycle of infinite period is only known to come into existence via a codimension-1 bifurcation in the ways described above, all of which involve global structures in the phase space in addition to the local saddle-node bifurcation.

IV. INADEQUACY OF SHADOW LIMIT ASYMPTOTICS

We now demonstrate the use of analytical tools from the literature to gain further insight into our numerical observations. We review and apply asymptotic movement of spike solutions in the Gierer-Meinhardt system due to spatial heterogeneity. Our objective is to demonstrate that these approaches, as they currently exist in the literature, are insufficient to explain the spatiotemporal oscillations.

In order to take advantage of the asymptotic analysis and its insight on spike localisation and movement, we

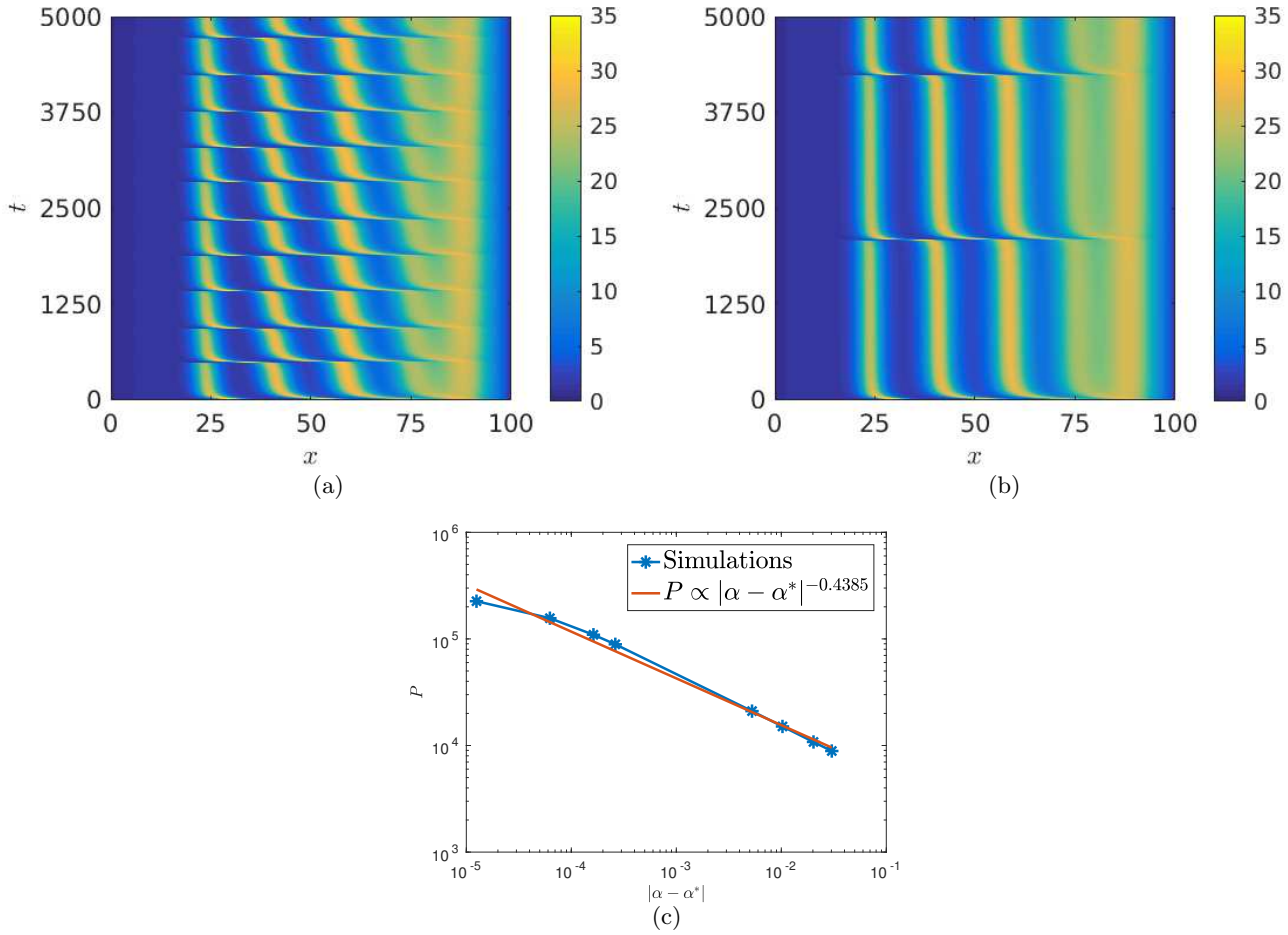

FIG. 8: Space-time plots of the activator u from solutions to Equations (2) in (a)-(b), and a plot of the period of the oscillations P against $|\alpha - \alpha^*|$ in (c). For all simulations we used $d = 10^4$, $L_x = 100$, $c_m = 0.8$, $\beta = 6$, and in (a) $\alpha = 1$, and (b) $\alpha = 1.125$. In all cases homogeneous Dirichlet boundary conditions are used (Color Figures available online).

transform the GM equations (1) into the form,

$$\frac{\partial a}{\partial \tilde{t}} = \epsilon^2 \nabla^2 a + \frac{a^2}{h} - \left(1 + \underbrace{\tilde{c}_m H\left(\frac{\xi+1}{2}\right)}_{V(\xi)} \right) a + \boxed{\epsilon \frac{r\alpha}{\mu}}, \quad \frac{\partial h}{\partial \tilde{t}} = D\nabla^2 h + \epsilon^{-1} a^2 - \underbrace{\left(\tilde{\nu} + \tilde{c}_n H\left(\frac{\xi+1}{2}\right) \right)}_{U(\xi)} h, \tag{3}$$

where we have rescaled with $t = \tilde{t}/\mu$, $\xi = (2x/L_x - 1) \in (-1, 1)$, $a = \epsilon u$, $h = v\epsilon\mu/r$, $\tilde{\nu} = \nu/\mu$, $\tilde{c}_m = c_m/\mu$, $\tilde{c}_n = c_n/\mu$, $D = \epsilon^2 d$, $\epsilon = 2/(L_x\sqrt{\mu})$.

We follow the one-spike asymptotic calculations from [14] to derive a differential equation determining the location $\xi_0(t)$ of the center of the one-spike solution. First, we calculate the inner solution (near the spike) and hence we introduce new variables $y = \epsilon^{-1}(\xi - \xi_0(\tau))$, $\tau = \epsilon^2 \tilde{t}$ and expand the functions h and a in an asymptotic series

$$h(y) = h_0(y) + \epsilon h_1(y) + \ldots, \quad a(y) = a_0(y) + \epsilon a_1(y) + \ldots,$$

for $\epsilon \ll 1$. We consider the time τ as a parameter and denote the spatial derivative with prime $()' = d/dy$.. The position $\xi_0(\tau)$ is chosen, without loss of generality, to satisfy $a'(0) = 0$. Collecting the leading order ($O(1)$) terms we obtain

$$a_0'' - (1 + V(\xi_0))a_0 + \frac{a_0^2}{h_0} = 0,$$
$$h_0'' = 0.$$

To be able to match the outer solution, h_0 cannot become unbounded as $y \to \pm\infty$ and hence we have $h_0 = K(\tau)$. Using this we simplify the equation for a_0 by rescaling with K and obtain

$$a_0(y) = K(\tau)\frac{3}{2}(1+V(\xi_0))\text{sech}^2\left(\sqrt{1+V(\xi_0)}y/2\right) \equiv K(\tau)u_c(y),$$

where $u_c(y)$ depends implicitly on τ, and is the unique solution to the differential equation,

$$u_c'' - (1+V(\xi_0))u_c + u_c^2 = 0, \tag{4}$$

satisfying $u_c'(0) = 0$, $u_c(0) > 0$ and which decays as $y \to \pm\infty$.

Instead of finding the leading order contribution to the outer solution, we inspect the next order, $O(\epsilon)$, inner solution. The reason for this is that this set of differential equations has a solution only if a solvability condition is satisfied. In particular, the Fredholm Alternative Theorem states that if an operator $\mathcal{L}$ is self-adjoint and the homogeneous problem $\mathcal{L}[u_H] = 0$ has a nontrivial solution u_H, then $\mathcal{L}u = F$ has solutions if and only if $\langle F, u_H\rangle = 0$, where $\langle\cdot,\cdot\rangle$ denotes the inner product with respect to which the operator $\mathcal{L}$ is self-adjoint.

The differential equations for $a_1,\ h_1$ are

$$a_1'' - (1+V(\xi_0))a_1 + 2\frac{a_0}{h_0}a_1 = \frac{a_0^2}{h_0^2}h_1 - \frac{\mathrm{d}\xi_0}{\mathrm{d}\tau}a_0' + yV'(\xi_0)a_0 - \frac{r\alpha}{\mu},$$

$$Dh_1'' = -a_0^2.$$

As with a_0 we rescale by letting $a_1 = K(\tau)u_1$, where u_1 satisfies,

$$\mathcal{L}(u_1) \equiv u_1'' - (1+V(\xi_0))u_1 + 2u_cu_1 = \frac{u_c^2}{K(\tau)}h_1 - \frac{\mathrm{d}\xi_0}{\mathrm{d}\tau}u_c' + yV'(\xi_0)u_c - \frac{r\alpha}{K(\tau)\mu}, \tag{5}$$

By differentiating equation (4), one can check that $\mathcal{L}[u_c'] = (\mathcal{L}[u_c])' = 0$ and hence we have a nonzero solution to the homogeneous problem. Therefore, the first subleading order equation has a solution only if the right-hand side of (5) is orthogonal to u_c', i.e.,

$$\left\langle \frac{u_c^2}{K}h_1 + yV'(\xi_0)u_c - \frac{r\alpha}{K(\tau)\mu}, u_c' \right\rangle = \frac{\mathrm{d}\xi_0}{\mathrm{d}\tau}\langle u_c', u_c'\rangle,$$

which is Equation (2.7) in [14], except for the α term. However, as u_c vanishes at $\pm\infty$ we observe that this additional term does *not* contribute to the solvability condition nor has it altered the spike profile to leading order. Finally, in the outer region, the concentration of a is exponentially small and hence the outer problem can be considered as only a problem for h_0 yielding a relation for the yet undetermined function K. Therefore, the dynamics of a single spike (the pinning evolution) remains unaffected by the α term according to the prediction of the asymptotic calculations and so the results found in [14] apply for any value of α such that spike solutions exist.

We now compare the asymptotics and numerics with an α that does not lead to spatiotemporal oscillations. For simplicity, consider the inhibitor kinetics without any heterogeneity, $c_n = 0$. Then the spike center, $x_0 \in (-1,1)$, follows the asymptotic relation given in Eq (2.19) from [14] for arbitrary D, which is given by

$$\frac{\mathrm{d}x_0}{\mathrm{d}t} = -\epsilon^2\sqrt{\nu/D}\left(\tanh\left[\sqrt{\nu/D}(1+x_0)\right] - \tanh\left[\sqrt{\nu/D}(1-x_0)\right]\right) - \frac{5\epsilon^2}{2}\frac{c_mH'(x_0)}{1+c_mH(x_0)}, \tag{6}$$

which is also numerically validated in [13, 14]. We compare this solution with our numerical solutions in Figure 9, and note that these solutions agree reasonably well with an isolated spot (Figure 9a), and a spike with one 'boundary' spike (Figure 9b), as long as $\alpha = 0$ so that no additional spikes spontaneously form. For $\alpha = 0.9$, the interaction of the spike solutions causes a disagreement with the analytics, but the overall speed is still reasonably well-approximated (Figure 9c). Finally, for a slightly larger value of the feed rate, $\alpha = 0.95$, we observe the spatiotemporal oscillation in Figure 9d.

The important part to note in Figure 9 is that while the speed of spike solutions matches the asymptotics, a slight change of the subleading parameter α from the value $\alpha = 0.9$ to 0.95 does not yield any change in the asymptotic predictions. However, this change ultimately destabilizes the spike and generates the spatiotemporal oscillations described in the preceding Sections.

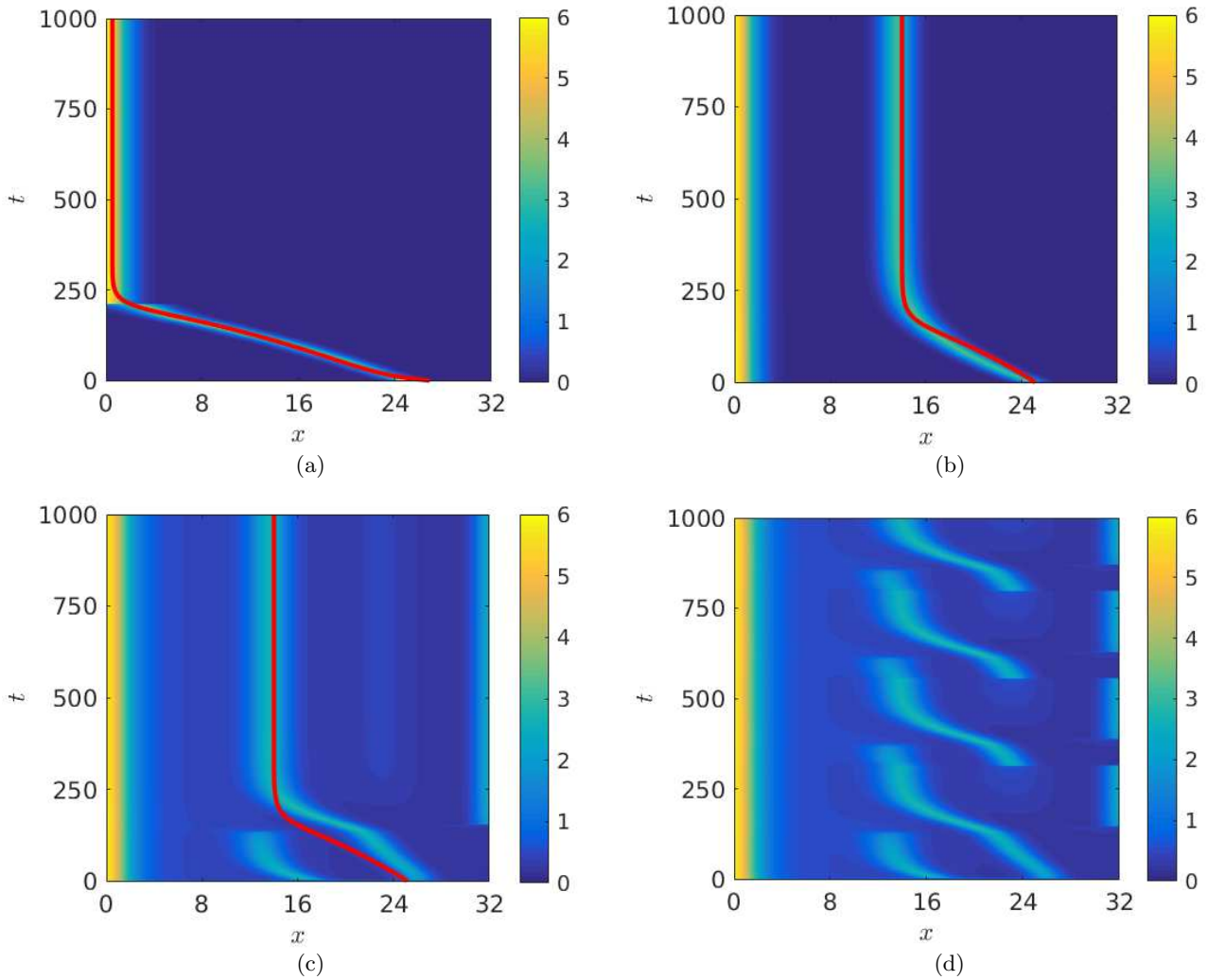

FIG. 9: Comparison of the analytical prediction and the numerical solution of (1) in a stationary parameter regime, where the analytical solution of x_0 is plotted as a red line. We take $L_x = 32$, $d = 55$, $r = 1$, $\mu = 1.6$, $c_m = 4.3$, $\nu = 3$, $c_n = 0$, and $\alpha = 0$ in (a)-(b), $\alpha = 0.9$ in (c), and $\alpha = 0.95$ in (d). In all cases Neumann conditions are used. In (a) and (d), generic random initial data are taken, whereas in (b) and (c) initial data are used, with the latter requiring $\alpha = 0$ in order to selectively generate the spike. Note that one cannot map $[0, L_x]$ directly to $[-1, 1]$ as the latter corresponds to the wavelength of the spike, so we have rescaled the asymptotic solution to agree with our numerical results as $t \to \infty$ (Color Figures available online).

V. INTERACTING HETEROGENEITIES AND EXCITABILITY

In this section, we analyse two additional aspects of this time-periodic phenomenon. We consider equations (1) for nonzero values of both c_m and c_n, with a linear heterogeneity $H(x) = x$, and show how varying both of these parameters leads to regions with and without oscillatory solutions. Near the boundary of this instability, before the saddle-node bifurcation described in Section III destabilizes the non-uniform steady state, we also explore how sensitive this steady state is to perturbations. We use COMSOL as described in Section II using 10^3 finite elements to facilitate many simulations of equations (1).

We first construct a bifurcation diagram depicting regions of non-stationary behavior, using parameters similar to Figure 6. To classify solution behaviors, we simulate equations (1) for $T = 2 \times 10^4$ units of time, and then extract the last 1/3 of the values of the activator u (using a time resolution of unity) at the midpoint of the domain, $x = L_x/2$. We then compute the coefficient of variation (standard deviation divided by the mean) of the time series given by $u(L_x/2, t)$ for t being the sequence of time points described above. We plot the result in Figure 10. We note that other

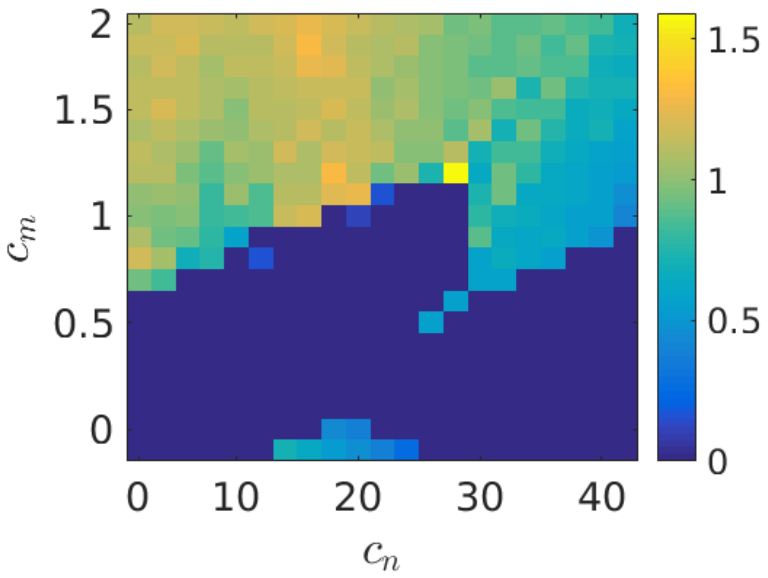

FIG. 10: Bifurcation plot of the coefficient of variation of $u(L_x/2, t)$ for t in the last 1/3 of the simulation time, as c_m and c_n vary. We take $c_n = 0, 2, 4, \ldots, 40$ and $c_m = 0, 0.1, 0.2, \ldots, 2$. We used $L_x = 100$, $d = 100$, $r = 1$, $\mu = 1$, $\nu = 4$, and $\alpha = 0.5$. The color scheme corresponds to the standard deviation of the value of u divided by its mean (in time). All nonzero values are oscillatory, with larger values indicating more variation in the time series of $u(L_x/2, t)$. In all cases Neumann conditions are used. (Color Figures available online).

alternatives (such as comparing maxima and minima of this data) give qualitatively the same diagram. This particular metric gives a notion of the overall variation in the time series of $u(L_x/2, t)$, which should correlate with both the amplitude and frequency of oscillations. More importantly, it clearly divides the parameter space into oscillatory and stationary regions.

For small values of c_n and c_m, solutions reach stationary steady states. As each of these is increased, we observe the oscillatory behavior described in the preceding sections. We see that the regions where this instability occurs are apparently disconnected, and non-convex. For instance, fixing $c_m = 0.8$, we see that $c_n = 0$ is oscillatory, $c_n = 4$ is stationary, $c_n = 30$ is oscillatory, and $c_n = 40$ is again stationary. We confirm these simulations, as well as solution behavior along the boundaries of the instability regions (including the 'islands' around $c_m = 0.7$ and $c_n = 24$), by running these simulations using finer meshes and performing convergence checks. Figure 10 demonstrates a wide range of complexity to the parameter space, but for brevity we leave a systematic parameter-dependent study to future work.

We now consider the sensitivity of the system to perturbations near the bifurcation. Specifically, we consider the non-uniform steady state which was numerically shown to be stable in Section III (for equations (1) with $c_n = 0$) for $\alpha = 0.348$, where the steady state is stable to small perturbations. We now perturb this steady state by adding normally distributed noise with zero mean and standard deviation σ across each spatial finite element; by linearity of a normal random variable, as σ is increased, the likelihood of a large perturbation increases. We then simulate the system forward in time, and for some values of the noise level σ observe the interior spike become unstable, and a new spike appear to take its place. This new spike travels from the right side of the domain to the left, as in Figure 9c.

We note that $u(L_x/2, t) \approx 0$ for the stable steady state. To detect the destabilization of this spike, we compute 100 realizations for varying values of σ, and count those which satisfy $\max_t(u(L_x/2, t)) > 1$, which indicates a spike moving across the midpoint, as in Figure 9c. We plot the percentage of such realizations across σ in Figure 11. We note that for $\sigma \leq 0.1$, none of the realizations satisfied the above condition, while for $\sigma \geq 0.55$, a vast majority of them did. We interpret the destabilization of a spike, and the subsequent movement of a new spike, as a large excursion in phase space from the steady state. This suggests that near the instability leading to spatiotemporal oscillations, the solutions can undergo large excursions depending on initial perturbations, indicative of an excitable system. Such

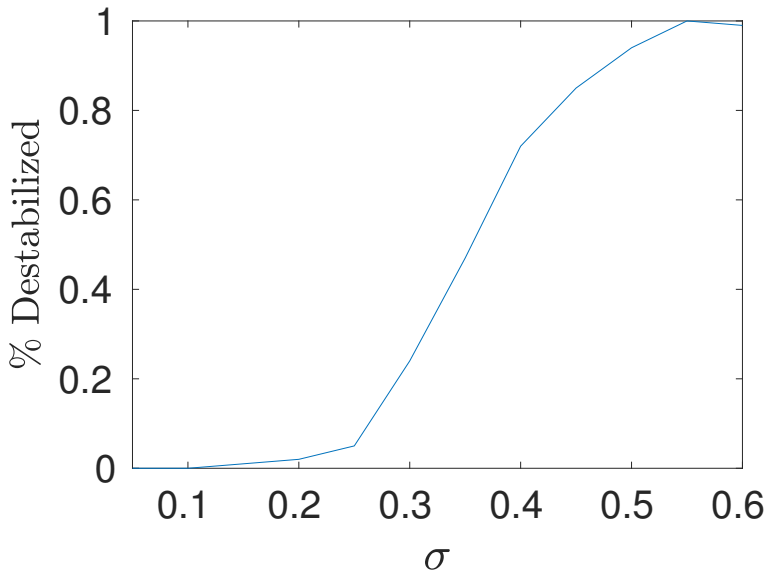

FIG. 11: Percentage of simulations which show destabilization of the non-uniform steady state as a function of the noise intensity of the perturbation, σ. We take $\sigma = 0, 0.05, 0.1, \ldots 0.6$, and use the same parameters as in Figure 6, except set $\alpha = 0.348$. Each value of σ was simulated for 100 different realizations, and a solution was deemed to be destabilized if $\max_t(u(L_x/2, t)) > 1$, indicating spike movement across the midpoint, as in Figure 9c (Color Figures available online).

excitability has been shown in a variety of physical systems, sometimes implicating large structures in the phase space such as in saddle-node-homoclinic bifurcations [44].

VI. DISCUSSION

We have demonstrated a complex spatiotemporal behavior induced in reaction-diffusion systems due to spatial heterogeneity. We have shown that this phenomenon appears robustly across a variety of reaction kinetics, and that while details of the system such as boundary conditions and forms of heterogeneity influence this behavior, it occurs for many specific instances of these systems. We also illustrate the importance of the 'open' nature of the systems we have investigated, whereby morphogens are fed exogenously into the system. This external production plays a crucial role in the bifurcation between stationary and oscillating solutions, and has been implicated in terms of robustness in patterning mechanisms in related models [45–47].

We used numerical simulations to determine the core properties of this phenomenon in Gierer-Meinhardt and Schnakenberg systems. We showed that for 'small' spatial heterogeneity and exogenous production, spike solutions form as is typical for large values of diffusion ratios, and these travel along the heterogeneity to reach a stable non-uniform configuration. Outside of these parameter regimes, however, we observe that this non-uniform steady state is no longer the globally attractive long-time behavior, and instead the movement of spikes across the domain leads to the destabilization of one spike, and the formation of a new one, together leading to a periodic traveling motion punctuated by destruction and creation of spikes.

We have shown that for a critical value of the basal production of activator in each system, the period of the oscillation diverges to infinity, and matches a power-law, although with non-universal exponents if the reaction kinetics are changed. This lack of universality suggests that the disappearance of the oscillatory behavior is not due to a canonical codimension-1 bifurcation, such as a bifurcation of a limit cycle with a homoclinic orbit or a Blue Sky Catastrophe. Additionally, the homogeneous steady state is Turing unstable, and local spike solutions are numerically predicted to disappear in saddle-node bifurcations as the oscillatory parameter regime is approached. As these are the only stable steady states in any nearby region of the parameter space, we conjecture that the oscillatory behavior is not generated from a local bifurcation of an equilibrium solution, but has a more complicated global dynamical origin. The non-canonical divergence of the period of this oscillation is also worthy of further investigation.

We explored the use of asymptotic methods for spike pinning present in the literature. These are able to capture the velocity of isolated spikes accurately, but are unable to elucidate any mechanism regarding the instability leading to the spatiotemporal behavior. We conjecture that it is the spike-spike interactions discussed in the numerical simulations that induce the punctuated spike destruction, driving the temporal dynamics. However, such non-local interactions require the consideration of exponentially small terms in non-stationary situations. This is beyond the current, though rapidly growing literature analyzing stability of multiple-spike solutions. We note that this literature includes spatially heterogeneous precursor gradients in Gierer-Meinhardt [15, 16, 48], as well as multi-spike solutions in Gray-Scott [49] and Schnakenberg [50].

Additionally, the continuation of stationary spike solutions reported in Section III suggests that these stability results will not give any insight into the spatiotemporal oscillations, as the spike solutions disappeared in a saddle-node bifurcation, which is not known to generate oscillatory dynamics (much less a limit cycle of divergent period). Hence, a more detailed analysis of global bifurcations in these models is needed. Such an analysis must account for both sources, such as the exogenous activator production α in (1), as well as spatial heterogeneity. We also note that the parameter space of these systems is complicated (Figure 10), suggesting that heterogeneity in different parts of a reaction-diffusion system have qualitatively different effects on observed dynamics. The behavior of spike solutions to noise near this bifurcation, shown in Section V, suggests the possibility of complex structure in the phase space, such as saddle-node and homoclinic bifurcations [44]. We leave further investigation of such possibilities as future work.

Finally, we remark that simulations of these systems in two spatial dimensions are typically more prone to this oscillatory behavior (e.g. we conjecture that the parameter space which is oscillatory is larger in two spatial dimensions, for suitable domain sizes and boundary conditions). This is likely due to a larger variety of stable configurations, and hence a more complicated phase space; see [16] for some discussion of the multistability of equilibrium solutions.

The ubiquity and robustness of these traveling patterns, as well as the difficulty in analyzing them, opens up many possibilities for further mathematical analysis to deepen our understanding of stability of far-from equilibrium dynamics of reaction-diffusion systems. This phenomenon also calls into question the use of Turing patterning mechanisms in realistic heterogeneous settings. As a small spatial heterogeneity, such as in Figure 4b, is able to prevent the emergence of a stable patterned solution, this shows that the Turing mechanism may be subject to further sensitivity preventing robust patterning. We view this development as a call to more clearly understand some of the structural and thermodynamic properties of reaction diffusion systems, and how realistic heterogeneities and exogenous inputs can lead to fundamentally different dynamical phenomena.

Acknowledgments

A.L.K. and E.A.G. are grateful for support from BBSRC grant BB/N006097/1; V.K. is grateful for support from the International mobility of researchers MSCA-IF grant CZ.02.2.69/0.0/0.0/17_050/0008025 funded by The Ministry of Education, Youth and Sports (MEYS) of the Czech Republic, as well as support from the Mathematical Institute at the University of Oxford. In compliance with BBSRC's open access initiative, the data in this paper is available from http://dx.doi.org/xxx/xxx.

[1] A. M. Turing. The chemical basis of morphogenesis. *Philosophical Transactions of the Royal Society of London. Series B, Biological Sciences*, 237(641):37–72, 1952.

[2] P. K. Maini, T. E. Woolley, R. E. Baker, E. A. Gaffney, and S. S. Lee. Turing's model for biological pattern formation and the robustness problem. *Interface focus*, 2(4):487–496, 2012.

[3] D. M. Holloway. *Reaction-diffusion theory of localized structures with application to vertebrate organogenesis.* PhD thesis, University of British Columbia, 1995.

[4] C. A. Cobbold, F. Lutscher, and J. A. Sherratt. Diffusion-driven instabilities and emerging spatial patterns in patchy landscapes. *Ecological Complexity*, 24:69–81, 2015.

[5] E. J. Crampin, W. W. Hackborn, and P. K. Maini. Pattern formation in reaction–diffusion models with nonuniform domain growth. *Bulletin of mathematical biology*, 64(4):747–769, 2002.

[6] D. Avitabile, V. F. Brena-Medina, and M. J. Ward. Spot dynamics in a reaction-diffusion model of plant root hair initiation. *SIAM Journal on Applied Mathematics*, 78(1), pp.291-319, 2017.

[7] V. F. Breña-Medina, D. Avitabile, A. R. Champneys, and M. J. Ward. Stripe to spot transition in a plant root hair initiation model. *SIAM Journal on Applied Mathematics*, 75(3):1090–1119, 2015.

[8] H. Meinhardt. Cell determination boundaries as organizing regions for secondary embryonic fields. *Developmental biology*, 96(2):375–385, 1983.

[9] K. D. Irvine and C. Rauskolb. Boundaries in development: formation and function. *Annual review of cell and developmental biology*, 17(1):189–214, 2001.

[10] D. L. Benson, J. A Sherratt, and P. K. Maini. Diffusion driven instability in an inhomogeneous domain. *Bulletin of mathematical biology*, 55(2):365–384, 1993.

[11] K. Page, P. K. Maini, and N. A. M. Monk. Pattern formation in spatially heterogeneous turing reaction–diffusion models. *Physica D: Nonlinear Phenomena*, 181(1):80–101, 2003.

[12] K. M. Page, P. K. Maini, and N. A. M. Monk. Complex pattern formation in reaction–diffusion systems with spatially varying parameters. *Physica D: Nonlinear Phenomena*, 202(1):95–115, 2005.

[13] D. Iron and M. J. Ward. Spike pinning for the gierer–meinhardt model. *Mathematics and computers in simulation*, 55(4):419–431, 2001.

[14] M. J. Ward, D. McInerney, P. Houston, D. Gavaghan, and P. Maini. The dynamics and pinning of a spike for a reaction-diffusion system. *SIAM Journal on Applied Mathematics*, 62(4):1297–1328, 2002.

[15] J. Wei and M. Winter. The gierer-meinhardt system with inhomogeneous coefficients. In *Mathematical Aspects of Pattern Formation in Biological Systems*, pages 149–173. Springer, 2014.

[16] J. Wei, M. Winter, and W. Yang. Stable spike clusters for the precursor gierer–meinhardt system in $\mathbb{R}^2$. *Calculus of Variations and Partial Differential Equations*, 56(5):142, 2017.

[17] V. Klika, R. E Baker, D. Headon, and E. A. Gaffney. The influence of receptor-mediated interactions on reaction-diffusion mechanisms of cellular self-organisation. *Bulletin of mathematical biology*, 74(4):935–957, 2012.

[18] J.-P. Voroney, A. T. Lawniczak, and R. Kapral. Turing pattern formation in heterogenous media. *Physica D: Nonlinear Phenomena*, 99(2-3):303–317, 1996.

[19] J. F. G. Auchmuty and G. Nicolis. Bifurcation analysis of nonlinear reaction-diffusion equationsi. evolution equations and the steady state solutions. *Bulletin of Mathematical Biology*, 37:323–365, 1975.

[20] S. T. A. Pickett and M. L. Cadenasso. Landscape ecology: spatial heterogeneity in ecological systems. *Science*, 269(5222):331–334, 1995.

[21] J. Clobert, L. Galliard, J. Cote, S. Meylan, M. Massot, et al. Informed dispersal, heterogeneity in animal dispersal syndromes and the dynamics of spatially structured populations. *Ecology letters*, 12(3):197–209, 2009.

[22] A. Warmflash, B. Sorre, F. Etoc, E. D. Siggia, and A. H. Brivanlou. A method to recapitulate early embryonic spatial patterning in human embryonic stem cells. *Nature methods*, 11(8):847, 2014.

[23] J. L. Aragón, R. A. Barrio, T. E. Woolley, R. E. Baker, and P. K. Maini. Nonlinear effects on turing patterns: Time oscillations and chaos. *Physical Review E*, 86(2):026201, 2012.

[24] W. Chen and M. J. Ward. Oscillatory instabilities and dynamics of multi-spike patterns for the one-dimensional gray-scott model. *European Journal of Applied Mathematics*, 20(2):187–214, 2009.

[25] H. Berestycki and F. Hamel. Generalized travelling waves for reaction-diffusion equations. *Contemporary Mathematics*, 446:101–124, 2007.

[26] M. M. Ayass, M. Al-Ghoul, and I. Lagzi. Chemical waves in heterogeneous media. *The Journal of Physical Chemistry A*, 118(50):11678–11682, 2014.

[27] N. Shigesada, K. Kawasaki, and E. Teramoto. Traveling periodic waves in heterogeneous environments. *Theoretical Population Biology*, 30(1):143–160, 1986.

[28] Y. Nishiura, T. Teramoto, X. Yuan, and K.-I. Ueda. Dynamics of traveling pulses in heterogeneous media. *Chaos: An interdisciplinary journal of nonlinear science*, 17(3):037104, 2007.

[29] P. van Heijster, A. Doelman, T. J. Kaper, and K. Promislow. Front interactions in a three-component system. *SIAM Journal on Applied Dynamical Systems*, 9(2):292–332, 2010.

[30] X. Yuan, T. Teramoto, and Y. Nishiura. Heterogeneity-induced defect bifurcation and pulse dynamics for a three-component reaction-diffusion system. *Physical Review E*, 75(3):036220, 2007.

[31] Rüdiger, S., Míguez, D., Munuzuri, A., Sagués, F., Casademunt, J. Dynamics of turing patterns under spatiotemporal forcing. Physical review letters 90 (12), 128301, 2003.

[32] Míguez, D. G., Pérez-Villar, V., Muñuzuri, A. P. Turing instability controlled by spatiotemporal imposed dynamics. Physical Review E 71 (6), 066217, 2005.

[33] Rüdiger, S., Nicola, E. M., Casademunt, J., Kramer, L., 2007. Theory of pattern forming systems under traveling-wave forcing. Physics Reports 447 (3-6), 73–111.

[34] X. Chen, R. Hambrock, and Y. Lou. Evolution of conditional dispersal: a reaction–diffusion–advection model. *Journal of mathematical biology*, 57(3):361–386, 2008.

[35] M. Dentz, T. Le Borgne, A. Englert, and B. Bijeljic. Mixing, spreading and reaction in heterogeneous media: A brief review. *Journal of contaminant hydrology*, 120:1–17, 2011.

[36] J. Ge, K. I. Kim, Z. Lin, and H. Zhu. A sis reaction–diffusion–advection model in a low-risk and high-risk domain. *Journal of Differential Equations*, 259(10):5486–5509, 2015.

[37] A. L. Krause, A. M. Burton, N. T. Fadai, and R. A. Van Gorder. Emergent structures in reaction-advection-diffusion systems on a sphere. *Physical Review E*, 2017. In Press.

[38] A. Gierer and H. Meinhardt. A theory of biological pattern formation. *Biological Cybernetics*, 12(1):30–39, 1972.

[39] K. A. Cliffe, A. Spence, and S. J. Tavener. The numerical analysis of bifurcation problems with application to fluid mechanics. *Acta Numerica*, 9:39–131, 2000.

[40] A. Ern and J.-L. Guermond. *Theory and practice of finite elements*, volume 159. Springer Science & Business Media, 2013.

[41] R. Seydel. *Practical Bifurcation and Stability Analysis*. Springer Science & Business Media, New York, December 2009.

[42] P. E. Farrell, C. H. L. Beentjes, and A. Birkisson. The computation of disconnected bifurcation diagrams. *arXiv preprint arXiv:1603.00809*, 2016.

[43] L. P. Shil'nikov. *Methods of qualitative theory in nonlinear dynamics*, volume 5. World Scientific, 2001.

[44] Krauskopf, B., Schneider, K., Sieber, J., Wieczorek, S., Wolfrum, M., 2003. Excitability and self-pulsations near homoclinic bifurcations in semiconductor laser systems. Optics Communications 215 (4-6), 367–379.

[45] D. Lebiedz and U. Brandt-Pollmann. Specific external forcing of spatiotemporal dynamics in reaction–diffusion systems. *Chaos: An Interdisciplinary Journal of Nonlinear Science*, 15(2):023901, 2005.

[46] J. C. Tzou and M. J. Ward. The stability and slow dynamics of spot patterns in the 2d brusselator model: The effect of open systems and heterogeneities. *SIAM Journal on Applied Dynamical Systems*, 16(1), 294-336., 2017.

[47] V. Breña-Medina and A. Champneys. Subcritical turing bifurcation and the morphogenesis of localized patterns. *Physical Review E*, 90(3):032923, 2014.

[48] J. Wei and M. Winter. Stable spike clusters for the one-dimensional gierer–meinhardt system. *European Journal of Applied Mathematics*, 28(4):576–635, 2017.

[49] W. Chen and M. J. Ward. The stability and dynamics of localized spot patterns in the two-dimensional gray–scott model. *SIAM Journal on Applied Dynamical Systems*, 10(2):582–666, 2011.

[50] T. Kolokolnikov, M. J. Ward, and J. Wei. Spot self-replication and dynamics for the schnakenburg model in a two-dimensional domain. *Journal of nonlinear science*, 19(1):1–56, 2009.